

Article

Bank Retreat and Streambank Morphology of a Meandering River during Summer and Single Flood Events in Northern Norway

Markus Foerst * and Nils R  ther

Department of Hydraulic and Environmental Engineering, Norwegian University of Science and Technology, 7031 Trondheim, Norway; nils.r  ther@ntnu.no

* Correspondence: markus.foerst@sweco.no; Tel.: +47-46891194

Received: 11 November 2018; Accepted: 6 December 2018; Published: 11 December 2018



Abstract: In recent years, advanced methods for measuring riverbank migration have been used to understand the process of river planform evolution. However, the role of the so-called outer secondary cell in the hydraulic pattern in bank erosion remains unclear. For this purpose, a natural river meander with high curvature bends and steep riverbanks was chosen to quantify bank migration by high-resolution terrestrial laser scanning of three patches along two river bends in four time intervals. The first two time intervals were seasonal, from spring to autumn, and with relatively few water level changes, whereas the third and fourth time intervals were short, just before and after single flood peak events. The yielded point clouds were filtered and digital elevation models (DEMs) were created. These DEMs were used to analyze bank retreat, riverbank morphology, and slope gradient changes in order to understand the role of the outer secondary cell in these processes. In addition, it is shown that storm events causing short peaks in river discharge are less important for river migration than longer-lasting medium discharge.

Keywords: outer cell; river migration; meander; erosion; meandering; outer secondary cell; ADCP; terrestrial laser scanner

1. Introduction

Riverbank migration has been investigated for decades and many approaches have been used to understand the process. These approaches can be divided into studies, for example, by scale, spatial resolution, and temporal resolution. Studies on large meandering rivers have been conducted by, for example, Parker et al. [1–3]. On the other hand, Schnauder and Sukhodolov have been working on river migration in small meandering rivers in Germany [4]. At the lower end of the scale, investigations of fluvial morphological processes on small-scale models in the laboratory have been conducted [5–9]. Finally, more sophisticated numerical models have appeared [10–12] in recent years.

In the last decade, measurement methods have been developed to estimate the sediment balance over short time scales [13]. One of these methods is erosion pins, and Lawler developed the most sophisticated ones [14]. These are able to measure and log sediment changes. However, they are intrusive [14–19] and their spatial resolution is within square decimeters. The use of light detection and ranging (LiDAR) in airborne surveys over large areas has been applied recently [20]. However, its application is limited when surveying vertical or near-vertical structures. This limitation can be overcome by using terrestrial LiDAR (terrestrial laser scanning, TLS). As a nonintrusive method, it avoids the physical impact of the measurement device at the investigated ground. Additionally, it collects a large amount of measurement points. The horizontal setup direction of the laser beam makes it perfect for riverbank surveys with a slope gradient higher than 45°. This setup results in

a dataset with a much higher resolution compared to, for example, the abovementioned erosion pins [21–25], and hence more detailed insight into the sediment balance of a riverbank [26]. This high resolution is necessary to measure small changes in riverbank morphology between flood events that occur within a short time interval. The investigated patches are small and have a very high point cloud density with a resolution beyond photogrammetry [27]. In addition, the analysis of laser scan time intervals gives insight into the processes of river migration that occur at a riverbank [23,28]. The limitation of TLS, however, is the lack of ongoing monitoring and the small area it is able to cover with high resolution.

A further phenomenon, the outer secondary cell, which was discovered and described for the first time by Thorne and Hey and Thorne et al. [29,30] some decades ago, recently came into focus again. Blanckaert recreated the conditions for the outer secondary cell in a flume [6,31]. Blanckaert and Graf explained a change in the downstream momentum due to a change in curvature [32]. Further investigation followed to analyze the outer secondary cell changes under different curvatures and depth-to-width aspect ratios [6,33–35]. However, the influence of an active riverbank was not a subject of their study. Foerst and R  ther investigated the hydraulics in the same river as this study by measuring the secondary flow direction along 72 transects [36,37]. At transects, where the outer riverbank was nearly vertical, they measured the outer secondary cell in a natural river directly. Thorne and Hey assumed that the outer secondary cell is a trigger for erosion at the outer bank [29]. However, Blanckaert and Graf described the outer secondary cell as forming a protective zone between the main secondary cell and the riverbank [32].

Mainly two kinds of erosion are described in the literature for river migration. The first is so-called erosion by fluvial entrainment [38]. This can be from groundwater seeping into the river, so-called seepage erosion, or from shear between the river and its channel, so-called fluvial erosion [10]. The other kind is mass failure or cantilever failure due to gravity [39–42]. The first erosion type happens slowly and continuously, while the second one occurs suddenly after the riverbank has been destabilized.

For this study, a medium-size river in the northern part of Norway was chosen to fill the gap between large-scale and small-scale investigations. The investigated parts of the riverbank were chosen to avoid influence by riparian vegetation. This paper investigates erosion by fluvial erosion in microscale and analyzes bank retreat and the shape of the streambank on a long-term (summer) and short-term (single flood event) basis with a terrestrial laser scanner as the high-resolution measurement method. The special focus herein is the role of the so-called outer secondary cell and its effect on fluvial erosion. This paper contributes to a better understanding of the role of the outer secondary cell in the interaction of river hydraulics and riverbanks by looking into the processes of bank retreat at microscale.

2. Materials and Methods

2.1. Study Site

The surveyed river, Breivikelva, is a lowland river in the northern part of Norway (Figure 1). The area was strongly affected by the last ice age, and a fluvial terrace system has since developed [38]. The chosen riverbanks for this study belong to the lowest terrace level, which is about 1–2 m above water level. The catchment covers an area of 164 km² with an altitude from 0 to 1400 m a.s.l. [43]. The investigated reach ends about 4.5 km before it discharges into the fjord. It is not influenced by tidal water changes. The river has a width-to-depth (W/D) ratio of 17, an average bed slope just less than 2%, and a sinuosity of around 3. The investigated reach is about 1100 m long and has an average energy slope of 0.4‰. The discharges measured within the study period vary between 8.7 m³s^{−1} in autumn and 24.3 m³s^{−1} in spring. The catchment of the study reach, 164 km², is relatively small; 58% lies over the tree line, while 0.7% of the area is covered by lakes. Consequently, the water level changes are strongly sensitive to rainfall events and snow melt due to temperature changes.

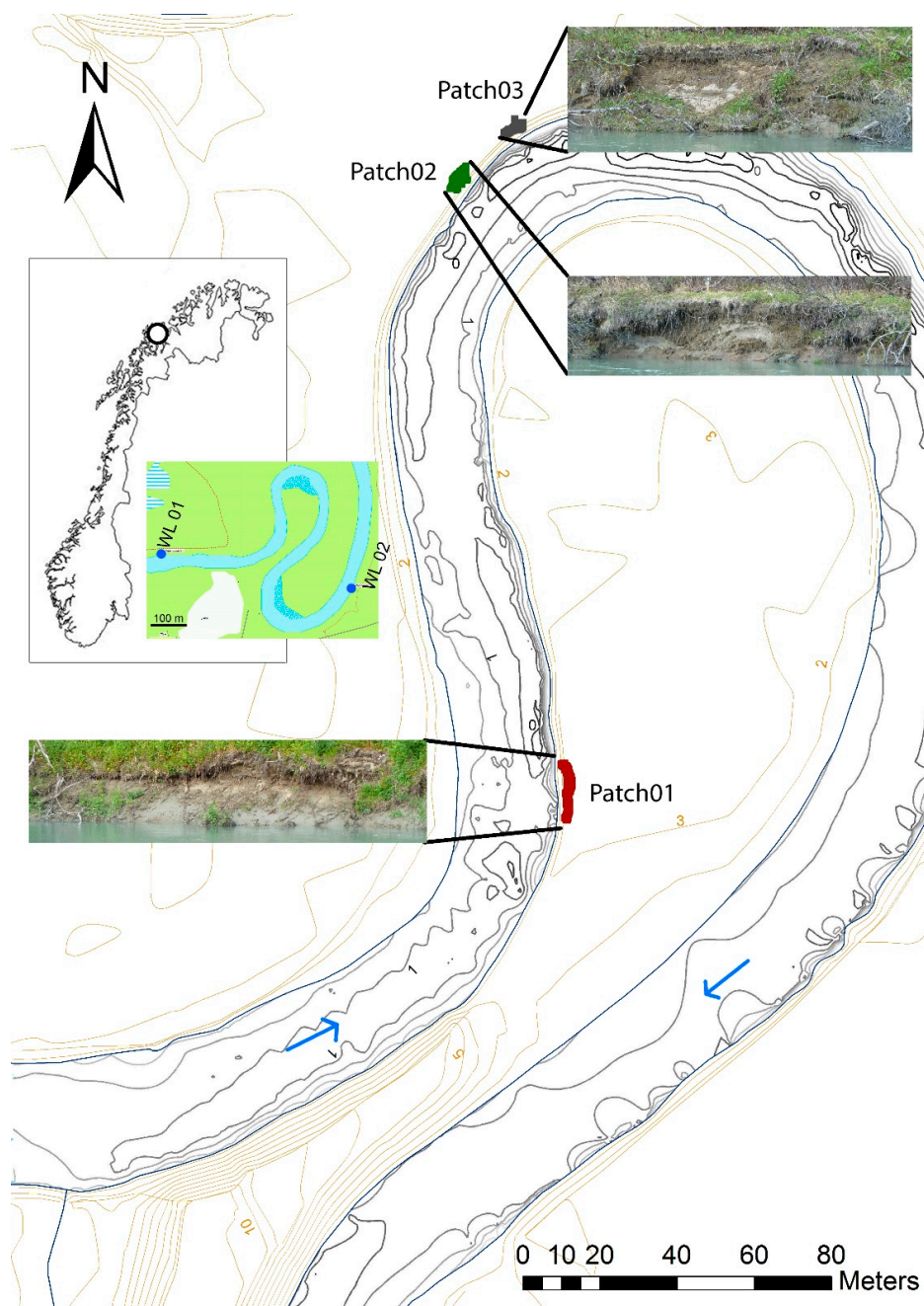


Figure 1. The investigated lowland river bend is located in the northern part of Norway. The flow is indicated by blue arrows. Investigated patches are shown at their locations. The locations of water level loggers are shown as WL01 upstream and WL02 downstream.

A meandering river can be divided into different sections along the bend: upstream of the bend apex, at the bend apex, and downstream of the bend apex [30]. Figure 1 shows the locations of the patches. They are all located at the outer side of the river bend. One is located downstream of the apex (patch 01) and two are located upstream of the apex (patches 02 and 03).

The river migrates through a valley filled with glaciofluvial sediments deposited since the end of the last ice age [39,40]. These deposits are thin undulating layers of sand and silt along the riverbank. A soil layer on top of the bank is thin and contributes little to stabilize the riverbank. The migration of the river through these deposits causes the formation of riverbanks up to 20 m high at the most downstream part of the investigated reach. The riverbed consists of both fine sand and coarse gravel.

Throughout the study reach, downstream fining can be observed. In the upstream part of the reach, the riverbed is armored so that gravels and cobbles dominate. Passing farther downstream, the armor layer disappears gradually and the riverbed consists of fine sand moving in ripples and dunes. The vegetation on the riverbanks consists of birch trees and vegetation patches (grass and moss), which fall and slide down the riverbank.

Following these parameters, the river can generally be classified after Rosgen to be an F-type river, which is described as an entrenched meandering riffle/pool channel on low gradients with a high width/depth ratio (study case: slope $S_w = 0.36\%$, $W/D > 20$). Specifically, it is an F4 river, since the bed material consists of sand and gravel [41]. According to Rosgen, an F4-type river has very high streambank erosion potential, but the influence of vegetation is only moderate. These criteria favor erosion by fluvial entrainment.

2.2. Data Acquisition

Several measurements were taken to investigate the bank erosion process at the study site. First, water level changes were recorded at the upstream and downstream ends of the reach (Figure 1). They were measured during May and August in 2011, June and October in 2012, and June and July in 2013. The fluctuation of water level showed a dependency on the amount of snow in the catchment. During spring and early summer, the water level rose with the course of the sun and the remaining snow in the mountains. This shows a certain influence of the amount of snow in the catchment on the hydraulics in the reach.

During 2011 and 2012, the measured water level fluctuated between 1.1 and 1.8 m a.s.l. downstream and 1.5 and 2.2 m a.s.l. upstream.

In spring 2013, the water level logger recorded one high-water event (2.3 m a.s.l.) after some days of rainfall from 23 to 27 June and a flood event at night from 3 to 4 July (Figure 2) at 2.55 m a.s.l. after heavy rain. The latter shows a rise in water level of about 60 cm within 4 h. The average discharge of the river during this three-season ongoing measurement campaign was about $9 \text{ m}^3 \text{ s}^{-1}$ at a water level of 1.4 m a.s.l.

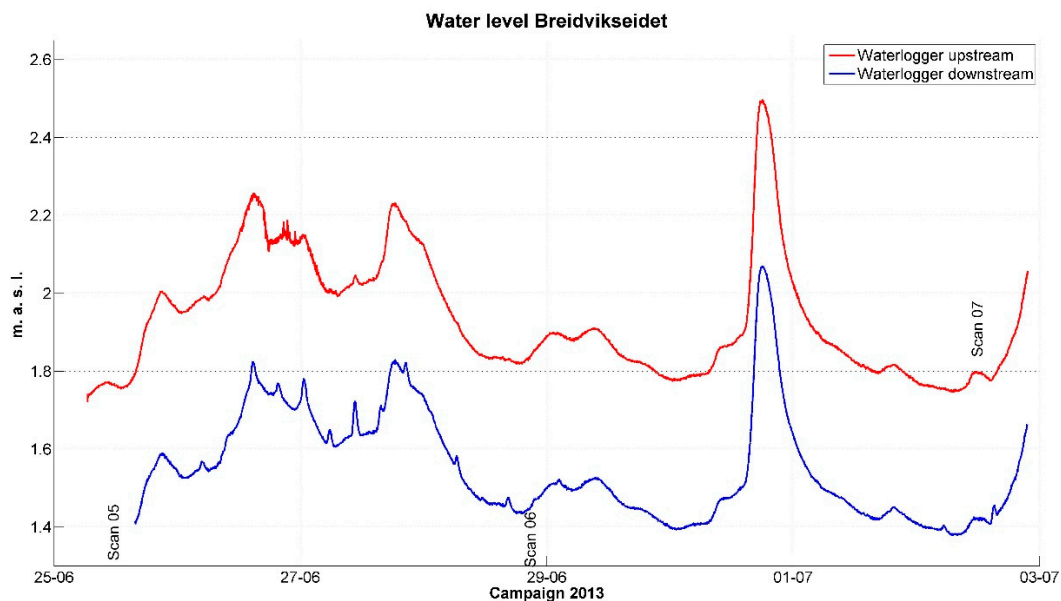


Figure 2. Water level during the third campaign as measured by the water loggers placed upstream and downstream.

Bathymetry was measured with a single beam echo sounder on an acoustic Doppler current profiler (ADCP) from Sontek (M9). The ADCP was directly coupled to a TopCon RTK-GPS (Real

Time Kinetic GPS) system. Foerst and R  ther described the campaign and the results in detail [37]. The bathymetry of the two meanders shows the typical pattern of the riverbed for flow through strongly curved and steeply sloped channels. As displayed in Figure 1, a steep outer bank and a mild gradient toward the inner bank characterize the profile of the cross section. Passing the end of the first meander bend, the riverbed flattens and becomes more symmetrical when the so-called crossover is passed. At the beginning of the second bend, a steep bank develops on the left side of the river. Analogous to the first river bend, a scour at the outer bank forms, causing a steep bank with a mild gradient toward the point bar.

In several field campaigns, the riverbank was scanned at six places along the outer banks to investigate longer-term and short-term processes. A TopCon GLS-1000 laser scanner with ScanMaster  software was used to conduct the scanning. The scanner was mounted on a tripod 1.5 m over the ground. The GLS-1000 operated with a Class 1 laser at 1535 nm. The accuracy of our measurement distance at <150 m was 4 mm under optimal conditions, which could be influenced by atmospheric conditions and the reflectivity of the scanned surface. The GLS-1000 was also equipped with a dual-axis compensator. Each outer bank was scanned from three scan positions in order to make sure that the parts lying in the shadow of one scan angle were covered by the other angles from the other positions. The scan distance was between 40 and 80 m. The three scan positions were combined by overlaying at least four georeferenced tie points. The target points were the same for each scan series and had to be removed between the scans. Therefore, a measurement error up to 0.010 m in the horizontal direction and 0.020 m in the vertical direction had to be taken into account. This target-based registration is the standard procedure (Sch urich et al., 2011). The mean error calculated by the ScanMaster  software was between 0.002 and 0.009 m, showing the high precision of the measurement method [42]. The georeferencing of the target point was done with a TopCon RTK-GPS system. The RTK correction came from a base station positioned on a known fixed point in the study area.

In 2011, these patches were scanned in May and June. Within this period, six rain events causing the water level to fluctuate strongly were recorded. In 2012, the same patches were scanned in June and October. During this period, the river discharge was strongly influenced by eight short rain events. During the field campaign in 2013, the periods between the three scans were shorter compared to the two previous ones. In total, three scans were taken with 10 days between the measurements. As can be seen in Figure 2, the hydrograph recorded in this period shows only one significant peak.

Additionally, in the investigated reach, a comprehensive dataset was taken, consisting of velocity and discharge measurements. Over 70 transects were measured with an ADCP under different hydraulic conditions. The analysis of the data gave valuable insight into the hydraulic conditions and the cross-sectional shapes prevailing at different flow stages and regimes (e.g., rather specific helical flow features in combination with steep riverbanks) [6]. These hydraulic features were observed independent of the prevailing flow stage. A detailed overview of these data is given in Foerst and R  ther [36].

2.3. Limitation of Method

The accuracy of the laser scan itself according to TopCon is a maximum at 4 mm from 1 to 150 m; this lies clearly within the measurement distance during this survey. The very low error during the overlay of the different scan angles confirms this assumption. Sch urich et al. showed in their study that the uncertainty rises with the complexity of the scanned landscape [42]. In this study, the scanned area is a nearly vertical riverbank. Therefore, it can be assumed that the data within one scan of the described patches are highly reliable. However, the GPS accuracy is between 0.008 and 0.013 m in the horizontal and between 0.012 and 0.017 m in the vertical direction. Experience has shown that GPS data are very constant within a dataset. That means that the offset for one set of measured target points is the same as long as the GPS system has reception from the satellites without long interruptions. This was again confirmed by the low mean error calculated during the scan overlay. The GPS error might be avoided if it is possible to leave the targets at the same position. This was not possible due to

the limited number of targets that were available. Another drawback is that the TLS scans were taken during different water levels (Table 1). The scans were therefore limited to the water surface and it was not possible to compare the total amount of sediment loss.

Table 1. Overview of scans and water level changes.

Scan	Date of Scan	Water Level m a.s.l.				Scan	Flood Events	Comment
		Min	Max	Mean	σ			
01	May 2011					1.84		Initial state
02	July 2011	1.67	2.38	2.02	0.28	1.64	8	After eight moderate high-water events
03	June 2012					1.58		Initial state
04	October 2012	1.35	2.16	1.95	0.16	1.26	6	After six moderate high-water events
05	19 June 2013					2.01		Initial state
06	28 June 2013	1.72	2.25	1.99	0.13	1.81	1	After one moderate high-water event over five days
07	6 July 2013	1.72	2.5	1.90	0.15	1.71	1	After one extreme high-water event

2.4. Data Postprocessing

2.4.1. Point Density Filtering and Digital Elevation Model (DEM)

This study focused on three positions along the first and second bends. These positions (patches 01–03) are shown in the plane view of Figure 1. The first patch was located at the end of the first river bend and the second and third patches were at the second river bend between inflow and apex. The patches were chosen because the heights of the riverbank have been the same and are located at the lowest level of the terrace system. Over the last three years, no considerable vegetation growth could be observed. The dimensions of the point clouds were defined by a vertical cut at 2.8 m a.s.l. as the upper limit. The lower limit was the water line at the moment when the scan was taken (Table 1). The point clouds showed single points, which have to be regarded as artifacts. These single points created during the scan were removed by a density filter. The basis of the filter was provided by the Point Cloud Library (PCL, 2013). The filter projected a sphere with radius R around each point and counted the number of points within this sphere. If there were a certain number of neighboring points N within this sphere, then it was defined as a good point; otherwise, it was regarded as an outlier [43,44]. The filter was applied with radius R from 0.01 to 0.15 m in steps of 0.015 m. The number of neighboring points was defined for $N = (5, 10, 5, 20, 25)$. Points with fewer than N neighbor points were deleted. In this way, for each point cloud, 50 filtered point clouds were created, and these point clouds were plotted. Afterward, they were visually inspected for whether enough outliers were removed and whether the point cloud was still coherent. The result was very different and no special pattern concerning the settings was visible. The final parameters used for the filtering are displayed in Table 2. Vegetation and dead wood, which blocked the view in front of the riverbank during the laser scans, were removed manually, first in the 2D view of ArcGIS© and then in the 3D view of ArcScene©.

Table 2. Results of filtering of terrestrial laser scanning (TLS) point clouds.

Scan	Date of Scan		Filter Parameter		Points Before Filtering	Points After Filtering	Points After Manual Cleaning	Water Level m a.s.l.			
			R	N				Min	Max	Scan	
Patch 01	01	May 2011	2011	0.055	15	79,735	60,252	59,151	1.67	2.38	1.84
	02	July 2011		0.025	5	52,678	36,305	35,618			1.64
	03	June 2012	2012	0.040	5	124,040	113,854	113,415	1.35	2.16	1.58
	04	October 2012		0.055	10	180,588	168,735	1,164,403			1.26
	05	19 June 2013	2013	0.040	5	286,670	270,056	269,707	1.72	2.25	2.01
	06	28 June 2013		0.025	5	379,610	351,198	339,921			1.81
	07	6 July 2013		0.040	5	566,067	549,132	523,337			1.71
Patch 02	01	May 2011	2011	0.040	15	94,658	91,164	91,145	1.67	2.38	1.76
	02	July 2011		0.040	5	26,579	23,992	23,949			1.72
	03	June 2012	2012	0.025	5	588,731	496,815	494,000	1.35	2.16	1.65
	04	October 2012		0.025	10	121,261	108,654	107,977			1.40
	05	19 June 2013	2013	0.040	10	886,871	824,974	818,160	1.72	2.25	1.60
	06	28 June 2013		0.040	10	147,365	130,180	129,223			1.77
	07	6 July 2013		0.025	10	445,743	430,526	425,447			1.76
Patch 03	01	May 2011	2011	0.040	5	41,569	26,706	26,665	1.67	2.38	2.03
	02	July 2011		0.040	10	27,570	20,741	20,741			1.73
	03	June 2012	2012	0.025	5	621,165	609,966	607,381	1.35	2.16	1.67
	04	October 2012		0.025	10	164,582	124,335	124,335			1.25
	05	19 June 2013	2013	0.040	10	907,733	887,744	887,409	1.72	2.25	1.60
	06	28 June 2013		0.040	15	109,946	99,567	98,975			1.80
	07	6 July 2013		0.040	20	297,441	242,797	239,662			1.71

2.4.2. Statistical Methods

For analysis of the DEM, patches 02 and 03 were virtually rotated so that the orientation was the same as patch 01, north-south. In this way, each row from the DEM displays the vertical extension and each column the horizontal extension. The vertical mean slope gradient and horizontal mean gradient were calculated by calculating the mean for each row and each column of the grid. In order to investigate the significance of slope change within a measurement period, the data were statistically verified. The slope gradient for each patch within a measurement period was compared, with the aim of verifying that the gradient between the scans was significantly different. To decide which statistical method was appropriate, the data needed to be tested for normal distribution. Therefore, the slope gradient for each patch was tested for normality with the Kolmogorov–Smirnov test. Since the slope gradient data were not normally distributed, the Kruskal–Wallis test was used to verify the significant difference between the slope gradients (Table 3).

2.4.3. Bank Retreat

The bank retreat was converted to a mass balance of sediments at the riverbank and was defined as the horizontal difference perpendicular to the shore line between successive scans. For this purpose, a DEM with a grid size of 0.05 m was created for each scan. The bank retreat was defined as the smallest distance between one point in the first scan and the surface to the consecutive scan; otherwise, there would be an overestimation of the retreat [17]. To estimate the bank retreat, for each grid cell, the horizontal distance to each grid cell was calculated at the same elevation a.s.l. of the successive scan. Then, the smallest value was used to define the retreat at each point. To avoid false data at positions where gaps in the point cloud existed, the maximum horizontal distance was set at 0.5 m. These grid cells, which had no corresponding grid cells within this distance in the second cell, were discarded. Finally, the total mass balance was calculated, and the volume change is given in m³ per horizontal square meter.

2.4.4. Slope Angle

From the filtered point cloud, a mesh was created with a cell size of 0.005 m. On this mesh, the point clouds were projected and a DEM was created. From this DEM, the slope gradient in degrees was calculated. The slope gradient ∇F is defined by

$$\nabla F = \frac{\partial F}{\partial x} \hat{i} + \frac{\partial F}{\partial y} \hat{j}$$

where \hat{i} and \hat{j} are standard unit vectors for the horizontal x and y coordinates.

Thus, the gradient in degrees (G_{deg}) was calculated with

$$G_{deg} = \text{atan}(\sqrt{(\nabla F_x)^2 + (\nabla F_y)^2}) \times \frac{180}{\pi}.$$

For the change in slope angle along the width of each patch, a mean vertical slope gradient (MVSG) was calculated. The MVSG is the average slope angle for each column in the grid of the DEM and the average slope at a given position along the riverbank. For the average slope angle, the mean value of all slope angles within the DEM was calculated.

3. Results

Riverbank Changes

Figure 3 shows the horizontal bank retreat at patch 02 between the scans over three years from a bird's-eye perspective in meters. The blue arrow indicates the direction of water flow. Positive numbers (red shades) mean retreat/erosion and negative numbers (blue shades) mean advance/sedimentation.

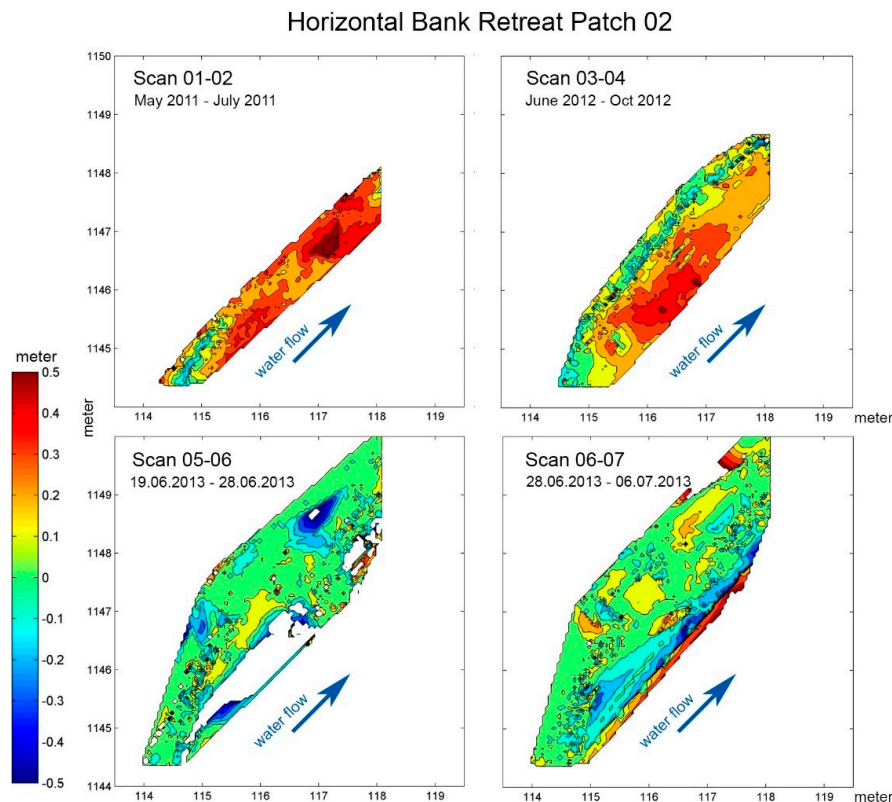


Figure 3. Horizontal bank retreat for patch 02 between scans.

Scans 01 and 02 in Figure 3 showed changes from May to July 2011. Between these scans, the water level alternated between 1.67 and 2.38 m, with eight peaks during that period. The mean water level was at 2.02 m a.s.l. Erosion took place nearly the whole way along the riverbank. The bank was stable or experienced a little sedimentation only during the first meter upstream. The erosion increased downstream. The average erosion was $0.31 \text{ m}^3/\text{m}^2$ (Table 3) and the slope angle changed from 52° to 40° .

Table 3. Change of riverbank. MVSG, mean vertical slope gradient, and significance of change with * $p < 0.05$ significant, ** $p < 0.01$ highly significant and *** $p < 0.001$ highly significant.

	Scan	Date of Scan	Average Slope Angle	Volume Change		Significance of Change
				Net	$\text{m}^3/\text{m}^2 =$ Meter Retreat	
Patch 01	01	May 2011	31.3°			***
	02	July 2011	32.7°	4.24	0.17	
	03	June 2012	32.5°	8.70	0.34	$p = 0.098$
	04	October 2012	34.2°	5.26	0.19	
	05	19 June 2013	39.9°	8.86	0.42	***
	06	28 June 2013	38.5°	3.99	0.11	
	07	6 July 2013	39.3°	2.97	0.09	$p = 0.446$
Patch 02	01	May 2011	52.0°			***
	02	July 2011	40.0°	1.14	0.31	
	03	June 2012	43.9°	1.60	0.28	***
	04	October 2012	38.2°	1.33	0.21	
	05	19 June 2013	51.5°	1.49	0.18	***
	06	28 June 2013	47.9°	0.11	0.01	***
	07	6 July 2013	49.2°	0.55	0.05	
Patch 03	01	May 2011	56.4°			***
	02	July 2011	44.6°	1.53	0.28	
	03	June 2012	47.4°	3.27	0.40	***
	04	October 2012	42.8°	0.82	0.11	
	05	19 June 2013	50.4°	-1.07	-0.17	***
	06	28 June 2013	47.3°	0.48	0.08	
	07	6 July 2013	48.2°	0.81	0.10	***

Scans 03 and 04 showed changes from June to October 2012. The water level alternated between 1.35 and 2.16 m with six peaks during that period. The mean water level was 1.95 m a.s.l. The highest erosion rates were in the middle part. The upper part along the patch did not experience erosion. The average slope angle changed from 43.9° to 38.2° and the average erosion was $0.21 \text{ m}^3/\text{m}^2$.

Scans 05 and 06 showed changes between 19 and 28 June 2013. During this period, there was only one high-water event with a duration of five days and two distinctive peaks (Figure 2). The water level alternated between 1.72 and 2.25 m a.s.l., with a mean water level at 1.99 m a.s.l. The patch showed little erosion. The average erosion was $0.01 \text{ m}^3/\text{m}^2$ and the average slope angle changed from 51.5° to 47.9° .

Scans 06 and 07 showed changes between 28 June and 6 July 2013. During this period, the highest flood event during the three-year field study occurred. The water level alternated between 1.4 and 1.5 m a.s.l. before and after the high peak and reached its maximum at 2.5 m a.s.l., while the mean water level was 1.9 m a.s.l. The patch showed hardly any erosion, except a narrow strip just above the water line. The color distribution shows increased erosion downstream. The average erosion was $0.05 \text{ m}^3/\text{m}^2$ and the average slope angle changed from 47.9° to 49.2° .

Table 3 compares all patches. The volume change showed similar patterns at all three patches. As seen in patch 02, the main erosion happened during lower water levels over a long time, three months in 2011 and four months in 2012. Little erosion happened during high-water events, as these happened twice in 2013. Patch 01 experienced 0.17 and $0.19 \text{ m}^3/\text{m}^2$ during the summer in 2011 and 2012, while in 2013, only $0.11 \text{ m}^3/\text{m}^2$ of erosion happened during one high-water event

over five days and as little as $0.9 \text{ m}^3/\text{m}^2$ during a short, severe high-water event at the end of the campaign. Patch 03 showed similar erosion behavior, with 0.28 and $0.11 \text{ m}^3/\text{m}^2$ retreat during summer 2011 and 2012, and only 0.08 and $0.10 \text{ m}^3/\text{m}^2$. However, the difference between the long-term and short-term events is not as clear as with patches 01 and 02; it shows less erosion after the short-term high-water event.

Thus, the retreat for each patch was not dependent on the size of the patch and was therefore comparable to each other.

Figure 4a–f shows the riverbank evolution from the side by showing a transect at the center part of each patch. Red lines show the riverbank in the beginning of the season and blue lines show the riverbank at the end of the season. As described previously, there were no changes during the flood events in 2013. Therefore, the cross sections for 2013 are not considered at this point. Table 3 shows the corresponding average slope angles.

Patch 01 showed an irregular slope in 2011 (Figure 4a). The upper part was slightly convex, and in the middle part, a step appeared. At the lower part, it had a 45° slope. Looking at the changes over time, it seems that the center of this patch advanced.

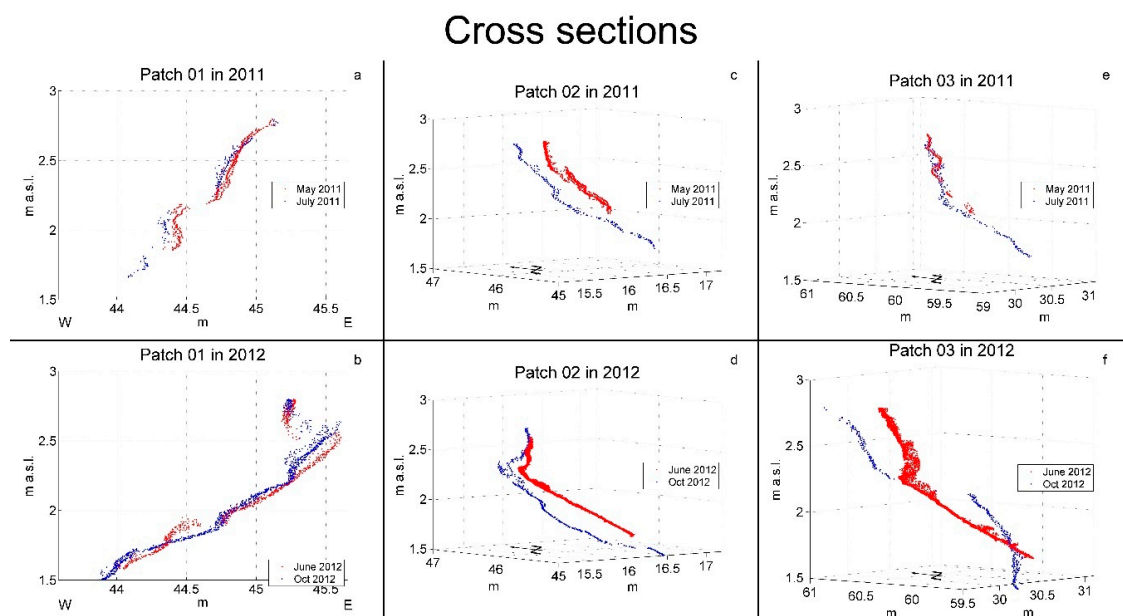


Figure 4. Cross sections of all three patches for the first and second measurement campaigns. Red lines show cross sections in the beginning of a campaign and blue lines show cross sections at the end. Changes for patch 01 are shown in (a,b), changes in patch 02 are shown in (c,d), and changes in patch 03 are shown in (e,f). The first letters (a,c,e) represent 2011 and the letters (b,d,f) represent 2012.

The year after (Figure 4b), patch 01 was characterized by an overhanging block and a mild downward slope. Looking at the changes over time, one can observe two major changes. One is that the overhang eroded partly and deposited just below. The other one is that in the lower third of the slope, material eroded and moved farther down the slope, while no changes were recorded in the middle part of the slope.

Patch 02 (Figure 4c) showed two different slope lines. The slope line from May was nearly vertical in the upper part, and after a breakpoint, the slope flattened. The slope line from July 2011 was not as steep in the upper part and flattened even more in the lower half. It had two distinctive steps, one just below the upper edge, and the second one at 2.1 m a.s.l. marking the change to the lower half. Patch 02 showed a clear bank retreat between May and July 2011.

In June 2012 (Figure 4d), the slope line changed. The upper part was nearly vertical at the top and had a straight slope with an angle below 45° at the beginning of the measurement in June. The scan in

October the same year showed a retreat below the top and had a concave slope toward the water line. The patch had no erosion at the top part, but showed clear bank retreat just below.

Patch 03 had a nearly vertical upper part and a less steep part farther down. The slope from May 2011 flattened downward, though the point where the flattening started was not clearly visible. On the other hand, the slope line from July showed a distinct break point at 2.1 m a.s.l. and flattened to an angle smaller than 45° . Patch 03 showed a stable steep part, while bank retreat occurred in the part below the break point.

In June 2012 (Figure 4f), the upper part had a convex, nearly vertical slope at the top and a straight slope with an angle below 45° at the beginning of the measurement in June. The scan from October in the same year showed a retreat at the upper part, where the convex slope changed to a straight slope. In the lower part, the straight slope changed to a convex slope. The transition points from convex to straight in June and from straight to convex in October were the same. Near the water surface, the slope from October became vertical. This patch showed in the upper part of the bank as retreat, in the middle part as sedimentation, and in the lowest part as retreat again.

For a better understanding of the mass distribution, the slope gradient was averaged in the vertical direction (Figure 5). The MVSG (Figure 5), plotted for each season and patch, describes the change of slope angle along the patch.

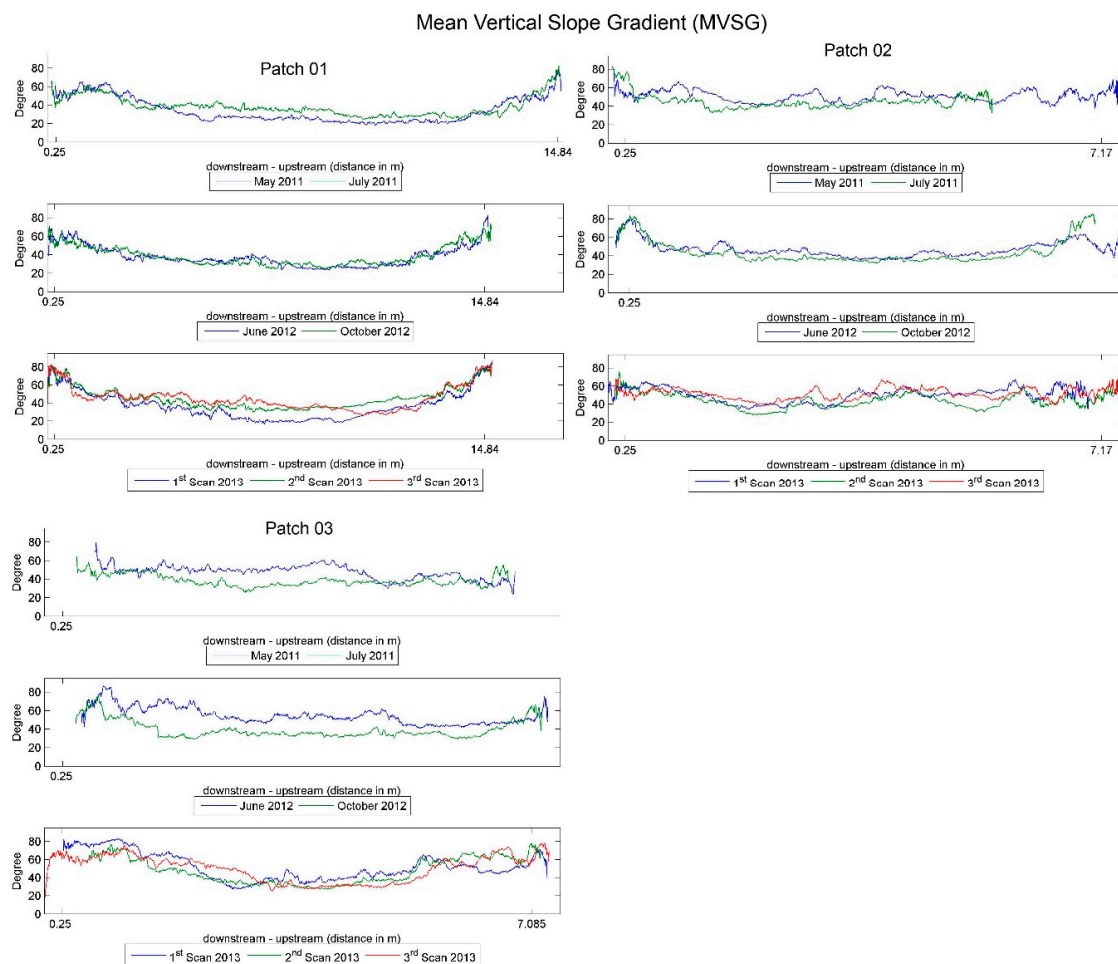


Figure 5. Change of mean vertical slope gradient for all patches during the study.

Patch 01 showed a steepening of the slope in the middle part from May to July 2011, while the edges did not change. In 2012, the June and October scans showed similar MVSGs along the patch. The analysis of the short-term scanning in 2013 showed an increase of MVSG at the middle part from

the first to the second scan. The change from the second scan to the third scan after the main flood event showed an increase of the slope angle downstream and a decrease upstream. The edges kept stable and did not show any change in slope angle during 2013.

The change of MVSG at patch 02 was not homogeneous over the width of the patch. It showed a general flattening between May and July 2011. In some small sections, around 1-m wide, no change of MVSG occurred at all, and in other sections, the change was more than 20° . The downstream edge showed a much steeper angle in July than in May. The following year, the slope became flatter equally over the length of the patch. However, the change of MVSG was much smaller, with a maximum around 10° . An exception was the upstream edge, where the slope got much steeper, from 45° to nearly vertical, while the downstream edge was stable. The short-term monitoring of patch 02 in 2013 showed a rather stable slope at the first quarter along the patch. The second middle part showed a flattening of the slope after the first flood event and a steepening after the main flood event. The slope after the main flood event was similar to the slope in the beginning of 2013.

Patch 03 for the first scan in 2011 showed a steep slope downstream ($\sim 60^\circ$). This changed upstream when the slope was below $\sim 40^\circ$. During the second scan, the slope was unchanged downstream but flattened over the whole length until it had about the same angle at the upstream part as in the beginning. The following season showed a similar pattern. In June, the slope angle was much steeper downstream ($\sim 80^\circ$ to 70°) and decreased upstream. The second scan showed steeper angles just in the beginning on the downstream side. After that, the slope was stable around 30° . The changes in 2013 were smaller. Between the first and second scans in 2013, patch 03 flattened in the downstream and middle sections, while it got steeper upstream. The change from the second scan to the third scan after the flood event showed steeper sections up- and downstream but hardly any changes in the middle part.

4. Discussion

This study focused on three patches located along the outside of two consecutive river bends. A retreat of the riverbank toward the outer side of the upper edge was measured at all three patches. The results show that the erosion rate was different at the three patches. Kleinhans discusses many interacting factors, such as vegetation, sediment, and climate, among others, that influence erodibility and, thereby, river channel formation. In the following, the results from this study are discussed in order to understand the reasons for the erosion and deposition patterns from the hydraulic point of view [44].

The following discussion is divided into two parts. The first part discusses the results of the first two observation intervals and the three locations, and the second part discusses the changes during the third and fourth intervals, which were significantly shorter.

Considering Figure 4 and Table 3, it can be seen that all three patches behaved according to the general understanding of bank erosion or retreat in meander bends. Looking at the details, one can see different erosional behavior for the different patches. Patches 02 and 03 behaved similarly but in a significantly different way compared to patch 01.

Patch 01 was located downstream of the apex in the most upstream bend. As can be seen in Figure 1, this bend had the lowest curvature compared to the other bends in this reach. Following Table 3, one can see that the average horizontal retreat of patch 01 was 0.17 m. This fell within the range of the measured values of the whole dataset. However, looking at Figure 4, this number seems contradictory to the obvious advance. One possible explanation for this behavior is that a block at this location started to rotate and had not yet failed.

Figure 4b illustrates the results of the measurement at the same patch the following year, during the period from June to October. The data from June show a significant overhang at the crest of the riverbank and accumulated material at the bottom of the slope. The data from October, represented by the blue line in Figure 4b, indicate that the crest partly collapsed and the material deposited in the

upper half of the slope. In addition, one can see that the accumulated material shown in the data of June was eroded.

The observed changes at the upper part of the slope during the campaign in 2011 as well as those during the campaign of 2012 can be classified as failure due to gravity, which is described in detail by Langendoen [8,25,28].

Following Figure 1, patches 02 and 03 were located in the second bend, which had significantly higher curvature compared to the first bend, where patch 01 was located. Patches 02 and 03 were situated just upstream of the apex of the second bend, with approximately 10 m in between.

The observed erosion process over time is characterized by three steps. First, one can observe a steepening of the riverbank (step I). At the second step (II), bank material falls from the top and accumulates in front of the bank toe. During the third step (III), this accumulated material is eroded, returning the riverbank back to its vertical shape, restarting the cycle in step I. Looking at Figure 4, it is now possible to identify when the measured changes occurred during the three steps. The changes in Figure 4c–e happened right after step II, where accumulated material starts to erode, while Figure 4f shows step II, where eroded bank material accumulates at the bank toe. In this context, the discussion is continued as to whether or not the outer secondary cell had a stabilizing effect on the riverbank. Experiments in the laboratory and field measurements have shown that as long as the riverbank is steep, outer secondary cells form [6,32,36,37]. Steep riverbanks are observed in step I of the described process, which leads to the assumption that the outer secondary cell, which dampens the boundary shear stress, prevents the riverbank from further erosion. The dampening of the boundary shear stress will then also lead to material originating from the riverbank accumulating at the bank toe, as described in step II of the process. At the end of step II, the deposited material has flattened the riverbank, and the outer secondary cell will disappear, so that the increased boundary shear stress will initialize erosion (step III). This is schematically illustrated in Figure 6.

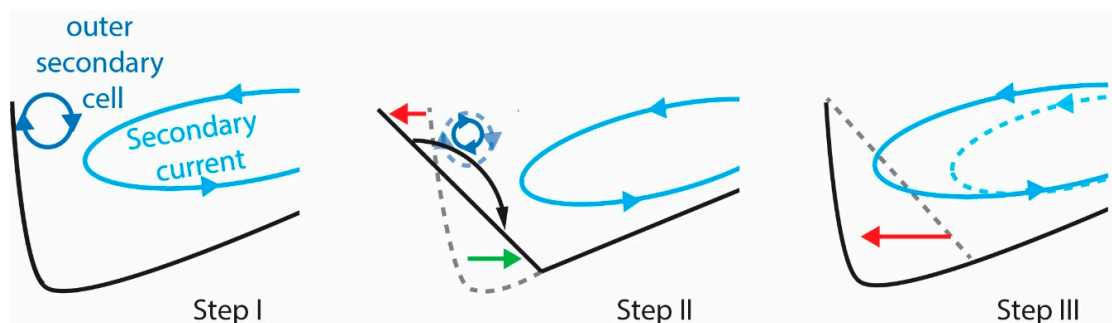


Figure 6. Schematic drawing of the three steps of the erosion process.

As can be seen from Figure 4, patches 02 and 03 behaved differently in the second time interval. This seems to be a contradiction, since they followed the same steps of the erosion process. A possible explanation can be that the location of the erosion process is dependent on the water level. Different discharge leads to a different water level and different hydraulic conditions. It is known from the literature that different hydraulic conditions lead to a relocation of the high-velocity cell as well as the strength level of the secondary current [45–47]. Therefore, the different behavior of patches 02 and 03 at the same measurement time interval was observed.

As a second part of the discussion, the analysis of changes during the third and fourth intervals is as follows. Compared to the first two observation intervals discussed above, the third and fourth are relatively short. As described in the previous section, the measured riverbank changes during these short observation intervals were not significant. However, the measured water levels recorded the maximum value within the total study time. The stable riverbank can be explained by the fact that the above-described process of the three steps was interrupted by the falling water level so that neither erosion nor deposition occurred. According to the hypothesis above, the outer secondary cell

dampened the boundary shear stress so that no material could be eroded (step I), and the short period of high water level prevented new material from depositing (step II).

5. Conclusions

This study focused on the erosional process and changes in the geomorphology of a riverbank triggered by river hydraulics. Herein, the riverbank of a lowland medium-size river was scanned with a terrestrial laser scanner in order to analyze the changes of bank geometry over time. The yielded point clouds were postprocessed by filtering for outliers, both automatically and manually. Based on these filtered data, the bank retreat and slope gradient were calculated. The Kruskal–Wallis test statistically tested the changes of the mean vertical slope gradient. It was possible to show which changes were highly statistically significant. This test proved to be a valuable tool to analyze point clouds for its difference in horizontal and vertical shapes. These results give insight into riverbank migration processes within an alternating water level over two summer seasons as well as migration processes within two short peak events. Hence, the sediment transport became clear.

The results lead to the following conclusions:

1. In the laboratory-observed phenomenon, the formation and existence of an outer secondary cell dampened the shear stress close to the riverbanks, and a possible consequence was observed and documented in a natural meandering river at bends with high curvature and relatively steep riverbanks. The dampening of the erosive behavior was documented by subsequent terrestrial laser scans of three patches along the riverbank.
2. This phenomenon could explain the stable riverbanks in short-peak events.
3. The location of the erosion process was dependent on the water level. Therefore, different erosional behaviors along one riverbank were observed simultaneously.

Author Contributions: M.F. and N.R. planned the fieldwork. The final research site was chosen by M.F. The laser scans were done by master's students under supervision by M.F. Point clouds were filtered with a script written by Aljoscha Sander. M.F. analyzed the data and verified them statistically. M.F. wrote the manuscript and N.R. reviewed it before submitting.

Funding: This research received no external funding.

Acknowledgments: We would like to thank Felix Hahn and Christian Mörtl, who carried out their master's and bachelor's studies, respectively, in the framework of this study. They contributed significantly to the success of this study. Their help during data acquisition and in handling the challenging logistics of the fieldwork is highly appreciated. A huge thank you also to Aljoscha Sander, who wrote a script for filtering of point clouds, which we were allowed to use.

Conflicts of Interest: The authors declare no conflict of interest.

References

1. Parker, G. *Stability of the Channel of the Minnesota River Near State Bridge No. 93, Minnesota*; University of Minnesota: Minneapolis, MN, USA, 1982.
2. Parker, G.; Diplas, P.; Akiyama, J. Meander bends of high amplitude. *J. Hydraul. Eng.* **1983**, *109*, 1323–1337. [[CrossRef](#)]
3. Parker, G.; Shimizu, Y.; Wilkerson, G.V.; Eke, E.C.; Abad, J.D.; Lauer, J.W.; Paola, C.; Dietrich, W.E.; Voller, V.R. A new framework for modeling the migration of meandering rivers. *Earth Surf. Proc. Land* **2011**, *36*, 70–86. [[CrossRef](#)]
4. Schnauder, I.; Sukhodolov, A.N. Flow in a tightly curving meander bend: Effects of seasonal changes in aquatic macrophyte cover. *Earth Surf. Proc. Land* **2012**, *37*, 1142–1157. [[CrossRef](#)]
5. Abad, J.D.; Garcia, M.H. Bed Morphology in Kinoshita Meandering Channels: Experiments and Numerical Simulations. In Proceedings of the 5th IAHR-Symposium on River, Coastal and Estuarine Morphodynamics, Enschede, The Netherlands, 17–21 September 2007; pp. 869–875.
6. Blanckaert, K. Secondary flow in sharp open-channel bends. *J. Fluid Mech.* **2004**, *498*, 353–380. [[CrossRef](#)]

7. Daly, E.R.; Miller, R.B.; Fox, G.A. Modeling streambank erosion and failure along protected and unprotected composite streambanks. *Adv. Water Resour.* **2015**, *81*, 114–127. [[CrossRef](#)]
8. Langendoen, E.J.; Simon, A.; Alonso, C.V. Modeling channel instabilities and mitigation strategies in eastern Nebraska. *Build. Partnersh.* **2000**. [[CrossRef](#)]
9. Farhadi, A.; Sindelar, C.; Tritthart, M.; Glas, M.; Blanckaert, K.; Habersack, H. An investigation on the outer bank cell of secondary flow in channel bends. *J. Hydro-Environ. Res.* **2018**, *18*, 1–11. [[CrossRef](#)]
10. Klavon, K.; Fox, G.; Guertault, L.; Langendoen, E.; Enlow, H.; Miller, R.; Khanal, A. Evaluating a process-based model for use in streambank stabilization: Insights on the Bank Stability and Toe Erosion Model (BSTEM). *Earth Surf. Proc. Land* **2017**, *42*, 191–213. [[CrossRef](#)]
11. Gu, L.; Zhang, S.; He, L.; Chen, D.; Blanckaert, K.; Ottevanger, W.; Zhang, Y. Modeling Flow Pattern and Evolution of Meandering Channels with a Nonlinear Model. *Water* **2016**, *8*, 418. [[CrossRef](#)]
12. Bosa, S.; Petti, M.; Pascolo, S. Numerical Modelling of Cohesive Bank Migration. *Water* **2018**, *10*, 961. [[CrossRef](#)]
13. Thomas, S. Review of methods to measure short time scale sediment accumulation. *Mar. Geol.* **2004**, *207*, 95–114. [[CrossRef](#)]
14. Lawler, D.M. Application of a novel automatic erosion and deposition monitoring system at a channel bank site on the tidal River Trent, U.K. *Estuar. Coast. Shelf Sci.* **2001**, *53*, 237–247. [[CrossRef](#)]
15. Couper, P.; Stott, T.; Maddock, I. Insights into river bank erosion processes derived from analysis of negative erosion-pin recordings: Observations from three recent UK studies. *Earth Surf. Proc. Land* **2002**, *27*, 59–79. [[CrossRef](#)]
16. Erlingsson, U. A sensor for measuring erosion and deposition. *J. Sediment. Petrol.* **1991**, *61*, 620–623. [[CrossRef](#)]
17. Haigh, M.J. The use of erosion pins in the study of slope evolution. *Br. Geomorphol. Res. Group Tech. Bull.* **1977**, *18*, 31–49.
18. Lawler, D.M. Advances in the continuous monitoring of erosion and deposition dynamics: Developments and applications of the new PEEP-3T system. *Geomorphology* **2008**, *93*, 17–39. [[CrossRef](#)]
19. Thorne, C.R. Field measurements of rates of bank erosion and bank material strength. In Proceedings of the IAHS Florence, Florence, Italy, 22–26 June 1981; pp. 503–512.
20. Milan, D.J.; Heritage, G.L.; Large, A.R.G.; Entwistle, N.S. Mapping hydraulic biotopes using terrestrial laser scan data of water surface properties. *Earth Surf. Proc. Land* **2010**, *35*, 918–931. [[CrossRef](#)]
21. Day, S.S.; Gran, K.B.; Belmont, P.; Wawrzyniec, T. Measuring bluff erosion part 1: Terrestrial laser scanning methods for change detection. *Earth Surf. Proc. Land* **2013**, *38*, 1055–1067. [[CrossRef](#)]
22. Day, S.S.; Gran, K.B.; Belmont, P.; Wawrzyniec, T. Measuring bluff erosion part 2: Pairing aerial photographs and terrestrial laser scanning to create a watershed scale sediment budget. *Earth Surf. Proc. Land* **2013**, *38*, 1068–1082. [[CrossRef](#)]
23. O’Neal, M.A.; Pizzuto, J.E. The rates and spatial patterns of annual riverbank erosion revealed through terrestrial laser-scanner surveys of the South River, Virginia. *Earth Surf. Proc. Land* **2011**, *36*, 695–701. [[CrossRef](#)]
24. Resop, J.P.; Hession, W.C. Terrestrial laser scanning for monitoring streambank retreat: Comparison with traditional surveying techniques. *J. Hydraul. Eng.* **2010**, *136*, 794–798. [[CrossRef](#)]
25. Wheaton, J.M.; Brasington, J.; Darby, S.E.; Sear, D.A. Accounting for uncertainty in DEMs from repeat topographic surveys: Improved sediment budgets. *Earth Surf. Proc. Land* **2010**, *35*, 136–156. [[CrossRef](#)]
26. Nasermoaddeli, M.H.; Pasche, E. Application of terrestrial 3D laser scanner in quantification of the riverbank erosion and deposition. In Proceedings of the International Conference on fluvial Hydraulics, Cesme-Ismir, Turkey, 3–5 September 2008; p. 10.
27. Brasington, J.; Vericat, D.; Rychkov, I. Modeling river bed morphology, roughness, and surface sedimentology using high resolution terrestrial laser scanning. *Water Resour. Res.* **2012**, *48*, 11. [[CrossRef](#)]
28. Jaboyedoff, M.; Demers, D.; Locat, J.; Locat, A.; Locat, P.; Oppikofer, T.; Robitaille, D.; Turmel, D. Use of terrestrial laser scanning for the characterization of retrogressive landslides in sensitive clay and rotational landslides in river banks. *Can. Geotech. J.* **2009**, *46*, 1379–1390. [[CrossRef](#)]
29. Thorne, C.R.; Hey, R.D. Direct measurements of secondary currents at a river inflexion point. *Nature* **1979**, *280*, 226–228. [[CrossRef](#)]

30. Thorne, C.R.; Zevenbergen, L.W.; Pitlick, J.C.; Rais, S.; Bradley, J.B.; Julien, P.Y. Direct measurements of secondary currents in a meandering sand-bed river. *Nature* **1985**, *315*, 746–747. [[CrossRef](#)]
31. Blanckaert, K. Mean flow and turbulence in open-channel bend. *J. Hydraul. Eng.* **2001**, *127*, 835–847. [[CrossRef](#)]
32. Blanckaert, K.; Graf, W.H. Momentum transport in sharp open-channel bends. *J. Hydraul. Eng.* **2004**, *130*, 186–198. [[CrossRef](#)]
33. Blanckaert, K. Hydrodynamic processes in sharp meander bends and their morphological implications. *J. Geophys. Res. Earth Surf.* **2011**, *116*. [[CrossRef](#)]
34. Ottewanger, W.; Blanckaert, K.; Uijttewaala, W.S.J. A parameter study on bank shear stresses in curved open channel flow by means of large-eddy simulation. *RCEM Proc.* **2011**, 1917–1927.
35. Van Balen, W.; Uijttewaala, W.S.J.; Blanckaert, K. Large-eddy simulation of a mildly curved open-channel flow. *J. Fluid Mech.* **2009**, *630*, 413–442. [[CrossRef](#)]
36. Foerst, M.; R  ther, N. Post Processing Methods of Moving Boat ADCP Measurements: Time Averaging vs. Distance Averaging. In *14. Treffen junger WissenschaftlerInnen an Wasserbauinstituten. Beitr  ge zum JuWi-Treffen am 25. und 26. Juni 2012 an der Technischen Universit  t M  nchen*; TU Munich: Munich, Germany, 2012; p. 216.
37. Foerst, M.; R  ther, N. Mean and Turbulent Flow Structures in two Consecutive Meander Bends. In *Proceedings of the IAHR Europe 2012, Munich, Germany, 27–29 June 2012*.
38. Langendoen, E.J.; Simon, A. *Stream Channel Evolution of Little Salt Creek and North Branch West Papillion Creek, Eastern Nebraska*; National Sedimentation Laboratory: Oxford, MS, USA, 2000.
39. Istanbuluo lu, E.; Bras, R.L.; Flores-Cervantes, H.; Tucker, G.E. Implications of bank failures and fluvial erosion for gully development: Field observations and modeling. *J. Geophys. Res. Earth Surf.* **2005**, *110*. [[CrossRef](#)]
40. Langendoen, E.J. CONCEPTS-Conservational Channel Evolution and Pollutant Transport System. In *Guideline NSL Technical Report*; Laboratory, U.-A.N.S.: Oxford, MS, USA, 2000; p. 180.
41. Langendoen, E.J. Modeling the Evolution of Incised Streams. II: Streambank Erosion. *J. Hydraul. Eng.* **2008**, *134*, 905. [[CrossRef](#)]
42. Patsinghasanee, S.; Kimura, I.; Shimizu, Y.; Nabi, M. Experiments and modelling of cantilever failures for cohesive riverbanks. *J. Hydraul. Res.* **2018**, *56*, 76–95. [[CrossRef](#)]
43. NVE. NEVINA. Available online: nevina.nve.no (accessed on 1 July 2012).
44. Kleinhans, M.G. Sorting out river channel patterns. *Prog. Phys. Geogr.* **2010**, *34*, 287–326. [[CrossRef](#)]
45. Abad, J.D.; Rhoads, B.L.; Guneralp, I.; Garcia, M.H. Flow structure at different stages in a meander-bend with bendway weirs. *J. Hydraul. Eng.* **2008**, *134*, 1052–1063. [[CrossRef](#)]
46. Kasvi, E.; Alho, P.; Lotsari, E.; Wang, Y.; Kukko, A.; Hyyp  , H.; Hyyp  , J. Two-dimensional and three-dimensional computational models in hydrodynamic and morphodynamic reconstructions of a river bend: Sensitivity and functionality. *Hydrol. Process* **2015**, *29*, 1604–1629. [[CrossRef](#)]
47. Nanson, R.A. Flow fields in tightly curving meander bends of low width-depth ratio. *Earth Surf. Proc. Land* **2010**, *35*, 119–135. [[CrossRef](#)]

